

# Non-Gaussian entanglement via splitting of a few thermal quanta

Pradip Laha,<sup>\*</sup> Darren W. Moore,<sup>†</sup> and Radim Filip<sup>‡</sup>

*Department of Optics, Palacký University, 17. listopadu 1192/12, 771 46 Olomouc, Czech Republic*

Quanta splitting is an essential generator of Gaussian entanglement, apparently the most commonly occurring form of entanglement in linearised systems. In general, such Gaussian entanglement results from the strong pumping of a nonlinear process with the highly coherent and low-noise external drive necessary for the linearisation. In contrast, recent experiments involving efficient trilinear processes in trapped ions and superconducting circuits have opened the complementary possibility to test the splitting of a few thermal quanta without a linearisation process. Stimulated by such small thermal energy, the strong degenerate trilinear coupling generates large amounts of nonclassicality, detectable by more than 3 dB of distillable quadrature squeezing, in contrast with the nondegenerate trilinear coupling. Substantial entanglement can be generated in tandem with the nonclassicality generation via linear coupling to a third mode, achieving the entanglement potential of the nonclassical states. Such entanglement, although not captured by the covariance matrix, grows with the mean number of split thermal quanta; something which does not happen with Gaussian entanglement. We extend our analysis to higher-order degenerate quanta splitting processes to demonstrate that this non-Gaussian entanglement is already common for strongly nonlinear systems at the low-energy thermal level. We thus shed light on the generic entanglement mechanism for nonlinear bosonic systems operating in such low-energy regimes.

*Introduction*— Entangled quantum harmonic oscillators form the backbone of many fields of quantum physics and applications in quantum technology. The most frequently occurring entanglement seems to be the Gaussian entanglement of weakly nonlinear systems, where a strong, coherent, and low-noise external drive is used to linearise nonlinear systems [1]. However, strongly nonlinear quantum interactions exhibit a much richer and exciting variety of phenomena which can potentially produce entanglement from low thermal energy, although typically at the cost of ease of detection, simple explanations and analytical descriptions. Such unexplored phenomena may stimulate **new** nonlinear optics experiments using second- and high-harmonic generation [2, 3], three and four wave mixing [4–6] or multiphoton Kerr processes [7, 8]. In the microwave domain, superconducting circuits may take advantage of the nonlinearity of Josephson junctions to generate parametric amplification [9], three-photon downconversion [10] and induce trilinear Hamiltonians (SNAILs) [11, 12] outside the rotating wave approximation. Among the growing number of such processes, entanglement might be much more common than anticipated and even appear more autonomously without the need for a strong, coherent, and low-noise external drive.

The mechanical motion of trapped atoms is an excellent candidate for a proof-of-principle investigation of such entanglement due to several properties: (i) the strong nonlinear coupling of highly linear mechanical oscillators, (ii) low damping and substantial shielding from ambient background noises and (iii) the potential scalability of the trapped atoms [13, 14]. For the mechanical motion of electrically trapped ions, the intrinsic nonlinearity of the Coulomb coupling can be leveraged into several multimode versions of a trilinear Hamiltonian [15] of

the type historically studied to investigate generalisations of squeezing to higher order moments [16]. Recently, such Hamiltonians, including fully degenerate, partially degenerate and nondegenerate interactions, were also achieved in superconducting circuits [10, 17]. Scalability and the ultimate removal of small parasitic nonlinearities in the individual oscillators is under successful development. The trapped ion versions of such Hamiltonians, both partially degenerate and nondegenerate, comprising two-mode and three-mode nonlinearities respectively, have been experimentally achieved [18] and shown to be effective for tasks such as quantum simulation [19] and quantum refrigeration [20]. These systems are particularly suitable for proof-of-principle studies of new instances of non-Gaussian entanglement and further exploitation.

In this Letter, we analyse the deterministic creation of generic non-Gaussian entanglement arising from the splitting of a few thermal quanta in trilinear interactions and increasing with an increase in thermal occupation. In order to produce sufficiently large entanglement of two oscillators modes, induced by few thermal quanta, there are necessarily three modes, with one thermal mode implementing the internal thermal driving while the remaining two, receiving quanta from the thermal energy via the nonlinear interaction, become entangled. We begin our discussion from the lowest order nonlinear interactions between linear oscillators, usually the most feasible in experiments. Nondegenerate trilinear couplings, while producing Gaussian entanglement under a classical pump [21], do not produce bipartite entanglement from a thermal pump among any combination of the modes [6, 22] (see Supplementary Material (SM) for details). Hence, we focus on a degenerate trilinear interaction generating significant nonclassicality from just a

few thermal quanta. Nonclassicality is qualitatively visible both in the discrete energy basis via Klyshko's criteria [23, 24] and quantitatively in the continuous variable basis, where it manifests via distillable squeezing surpassing the 3dB limit [25]. It is remarkably robust, remaining detectable both by Klyshko's criteria and distillable squeezing despite an initial thermal occupation greater than one phonon in the degenerate mode. When the degenerate interaction is continuously combined with a linear coupling to an auxiliary mode the resulting non-Gaussian enhancement of logarithmic negativity can unconditionally reach  $\sim 0.77$ , saturating the entanglement potential of the nonclassical states. Non-Gaussian entanglement thus materialises straightforwardly via splitting of a few thermal quanta in a regime very different to the Gaussian regime involving a strong coherent pump. To make this attractive for proof-of-principle tests, we navigate towards possible experimental tests with trapped ions, or other alternative platforms, leaving the details for further experimental evaluation.

*Trilinear Hamiltonians with Trapped Ions*— A pair of ions with equal mass  $m$  and charge  $e$ , contained in a harmonic trap, are coupled via the Coulomb interaction. If the radial trapping frequencies  $\omega_x$  and  $\omega_y$  are assumed to be much greater than the axial trapping frequency  $\omega_z$ , then the ions distribute themselves along the  $z$ -axis with equilibrium positions  $(0, 0, z_i^0)$  [26], where  $z_1^0 = -\sqrt[3]{\frac{e^2}{4m\omega_z^2}} = -z_2^0$ . The Coulomb interaction can be expanded to second order, inducing a natural transformation to the normal modes of the motion, wherein the collective vibrational modes are decoupled from each other. The first step beyond this harmonic approximation, involving third order terms in the expansion, removes the decoupling of the spatial motion leading to interactions involving both the radial and axial modes. Components of these nonlinear interactions are resonant properties of the collective motion of the ions.

Recent experiments have achieved regimes in which these higher order interactions become relevant. The third order term in the Coulomb potential expansion is expressed, with  $Q_\alpha = \frac{1}{2}(r_{1\alpha} - r_{2\alpha})$  the relative position for axes  $\alpha = x, y, z$ , as

$$V^{(3)} = \frac{e^2}{4|Q_0|^4} Q_z (3(Q_x^2 + Q_y^2) - 2Q_z^2), \quad (1)$$

where  $Q_0 = \frac{1}{2}(z_1^0 - z_2^0)$ . Evidently, the relative motion of the ions becomes anharmonic and, importantly, the axial motion becomes coupled to the radial motion. From here, we will assume that the most significant components of the potential are those contributing to the interaction between the  $x$  and  $z$  spatial components. In this approximation, the potential energy can be expressed as

$$V \approx \sum_{\alpha=x,z} m\Omega_\alpha^2 Q_\alpha^2 + \frac{3e^2}{4|Q_0|^4} Q_z Q_x^2, \quad (2)$$

where we have defined the normal mode frequencies  $\Omega_x^2 = \omega_x^2 - \frac{e^2}{4m|Q_0^0|^3}$  and  $\Omega_z^2 = \omega_z^2 + \frac{e^2}{2m|Q_0^0|^3}$ . Alternatively for superconducting circuits trilinear interactions using SNAIs [11] can be considered to reach Eq. (1).

The motional variables can be quantized by promoting them to operators satisfying the canonical commutation relations  $[\hat{Q}_\alpha, \hat{P}_\alpha] = i\hbar$ , where  $\hat{P}_\alpha$  is the momentum operator corresponding to the normal mode  $\hat{Q}_\alpha$ . The canonical variables of the relative motion can be linked to annihilation operators by the relations  $\hat{Q}_z = \sqrt{\frac{\hbar}{2m\Omega_z}}(\hat{a} + \hat{a}^\dagger)$  and  $\hat{P}_z = i\sqrt{\frac{\hbar m\Omega_z}{2}}(\hat{a}^\dagger - \hat{a})$ , and  $\hat{Q}_x = \sqrt{\frac{\hbar}{2m\Omega_x}}(\hat{b} + \hat{b}^\dagger)$  and  $\hat{P}_x = i\sqrt{\frac{\hbar m\Omega_x}{2}}(\hat{b}^\dagger - \hat{b})$ , with  $[a, a^\dagger] = [b, b^\dagger] = \mathbb{I}$ . Expanding  $V$  in terms of the annihilation operators and moving to a frame rotating with the respect to the free motion generates an interaction Hamiltonian  $H$  of the form

$$H = \frac{3e^2}{4|Q_0|^4} (ae^{-i\Omega_z t} + a^\dagger e^{i\Omega_z t}) \times (b^2 e^{-i2\Omega_x t} + b^{\dagger 2} e^{i2\Omega_x t} + b^\dagger b + 1). \quad (3)$$

When  $\Omega_z = 2\Omega_x$ , several terms become resonant and in the rotating wave approximation the interaction Hamiltonian takes the trilinear form

$$H = \Omega_T (ab^{\dagger 2} + a^\dagger b^2), \quad (4)$$

where  $\Omega_T = \frac{3e^2}{4|Q_0|^4}$ . For a more detailed Hamiltonian analysis see, for instance, Refs. [26, 27]. This is a partially degenerate trilinear interaction in which the creation (annihilation) of a phonon in the axial direction results in the annihilation (creation) of a pair of phonons in the radial direction.

*Thermally Induced Nonclassicality and Non-Gaussian Entanglement*— The quanta splitting and ensuing nonclassicality from the nonlinear dynamics may proceed from a small amount of classical thermal noise present in one of the subsystems. By initialising the axial ( $a$ ) or radial ( $b$ ) components of the motion in thermal states while the remainder is initialised in the ground state, the degree to which the nonlinearity converts the initial resource of thermal noise into nonclassical behaviour can be examined (Fig. 1). In general, if the radial mode is used as a thermal pump of the axial mode then the nonclassicality and corresponding entanglement potential is small. In contrast, our starting point is that  $a$ , using the small incoherent energy of a thermal pump, can drive nonclassicality in  $b$ .

In the ideal case, the nonclassicality of mode  $b$  can be immediately seen from the phonon distribution  $P_k = \langle k|\rho|k\rangle$ ; the reduced state of mode  $b$  is nonclassical due to its population of only even Fock states irrespective of the strength of the thermal pump. This is verified directly by Klyshko's criteria [23, 24], which are automatically satisfied for odd number occupations and satisfied strongly

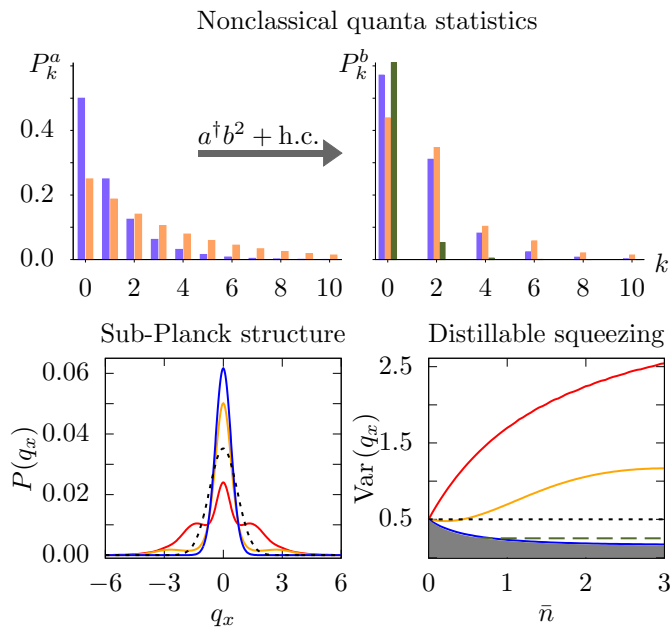


Figure 1. The upper panels demonstrate the production of nonclassicality due to thermal quanta splitting. Mode  $a$  is coupled to mode  $b$  through the trilinear coupling given by Eq. (4). Initially,  $a$  is in a thermal state (upper left) with mean thermal energy  $\bar{n}$ , while  $b$  is in the ground state (for thermal occupation of  $b$ , see SM). Thermal quanta in mode  $a$  are dynamically split into pairs in mode  $b$ , which generates nonclassical phase-insensitive phonon statistics (upper right), verified by Klyshko's criteria [23, 24]. Furthermore, increasing  $\bar{n}$  makes the nonclassical effects more pronounced. Purple and orange correspond to  $\bar{n} = 1$  and 3, respectively, while green corresponds to a squeezed state with 3 dB of squeezing. The nonclassicality of mode  $b$  after the trilinear interaction can also be quantified in a phase sensitive manner via distillable squeezing. The probability densities  $P(q_x)$ , of the dimensionless quadrature  $\hat{q}_x = \frac{b+b^\dagger}{\sqrt{2}}$ , are compared on the lower left for the ground state (dashed black) and with thermally induced nonclassicality,  $\bar{n} = 3$ , (red) demonstrating the sub-Planck structure around the origin generated by the nonlinear interaction. The yellow curve indicates the probability distribution of the distillable squeezed state close to the asymptotic limit, corresponding to the yellow curve in the lower right panel. Universal distillation of squeezing from multiple copies of the nonclassical state in mode  $b$  is shown on the lower right, with the asymptotic limit in grey [25] and the 3 dB squeezing limit in dashed green. Consuming progressively more copies produces a variance moving towards and then below the shot-noise level (dashed black). The distillation procedure saturates (blue), limited by the nonclassicality present in mode  $b$  after the trilinear interaction. Note, we have selected the time to coincide with the first peak of the entanglement dynamics.

for even occupations close to the peaks of the distribution. The nonclassicality is phase insensitive, reflecting the incoherent phase of the thermal pump (see SM for comparison with a coherent pump). Simultaneously, the non-Gaussian position probability density, despite hav-

ing a variance greater than the ground state, displays sub-Planck structure [28] around the global maximum verified by the presence of universally distillable squeezing [25], with the degree of squeezing available increasing with the thermal energy. Notably, despite the presence of such sub-Planck structures the Wigner function is positive at the level of the nonclassical state of  $b$ . The lower right panel of Fig. 1 shows that the degree of distillable squeezing due to quanta splitting is stimulated by  $\bar{n}$  beyond 3 dB. Remarkably, these nonclassical aspects are observable also for an initial thermal occupation of  $b$  larger than a single quantum (see SM).

The amount of nonclassicality capable of being converted to entanglement in a particular mode can be further characterised through the entanglement potential (EP), denoted  $\mathcal{E}$  [29]. The EP of mode  $a$  or  $b$  is evaluated through its capacity to become entangled via passive interactions with the ground state of an oscillator. This can be quantified by determining the logarithmic negativity (LN) [30], of the following state:

$$\rho_{\mathcal{E}} = U_{\text{BS}}^\dagger (\rho \otimes |0\rangle\langle 0|) U_{\text{BS}}, \quad (5)$$

where  $U_{\text{BS}} = e^{\frac{\pi}{4}(c^\dagger A - cA^\dagger)}$ , where  $c$  is an auxiliary mode prepared in the ground state,  $A = a, b$  and  $\rho$  is the reduced state corresponding to the mode  $A$ .

The nonclassicality converted from the thermal noise resource can be leveraged to create entanglement with another mode  $c$  which interacts simultaneously with  $b$  via the simple linear interaction

$$H_{\text{aux}} = H + g(bc^\dagger + b^\dagger c). \quad (6)$$

In our analysis, we have selected  $g = \Omega_T$ , which appears to give the best performance. Deviation from equality simply results in reduced LN, although the qualitative effects remain the same. Note that the beamsplitter coupling in Eqs. (5,6) in our case is incapable of generating any amount of entanglement from classical states. The entanglement is not a short-term effect, in the sense that it arises after an initial quiescent period in the dynamics, and optimisation of the interaction time necessarily occurs over anharmonically oscillating dynamics (see SM). To compromise we select the first peak of EP in order to balance finding significant entanglement while remaining closer to the short times available to experimental settings, where decoherence will be relevant.

The EP generated in  $b$  by a thermal pump in  $a$  is shown in Fig. 2 as the blue line. As a signature of nonclassicality, this is connected to the previous discussion of distillable squeezing by noting that if the non-Gaussian state with large EP is used to distill a Gaussian squeezed state (in the asymptotic limit), then this squeezed state generates similar EP to the non-Gaussian state from the trilinear interaction (black line). By introducing an auxiliary mode  $c$ , as in Eq. (6), the resulting LN, denoted  $\mathcal{L}_{b,c}$ , dynamically fulfills the EP of  $b$  as the red line in

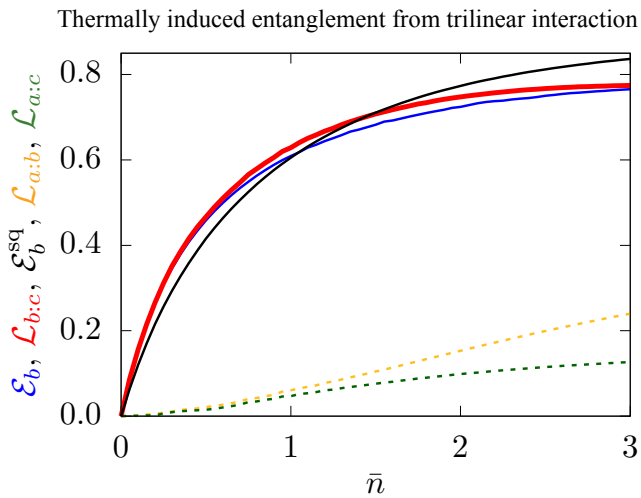


Figure 2. For the trilinear coupling given by Eq. (4), the entanglement potential  $\mathcal{E}_b$  (blue) of mode  $b$  generated by the thermal noise in  $a$  increases as the noise is increased. In the presence of a linear coupling Eq. (6) to an auxiliary mode  $c$ , we show the logarithmic negativity  $\mathcal{L}$  between  $b$  and  $c$  (red),  $a$  and  $b$  (yellow), and  $a$  and  $c$  (green).  $a$  is initially in a thermal state while  $b$  and  $c$  are initially in their respective ground states. The values plotted here correspond to the first peak in the temporal evolution of their respective quantities  $\mathcal{E}$  and  $\mathcal{L}$  which otherwise undergo rather complex evolution.  $\mathcal{L}_{bc}$  closely mimics the behavior of  $\mathcal{E}_b$  indicating that the entanglement potential of  $b$  can be realised dynamically, despite residual entanglement among the remaining modes.  $\mathcal{E}_b$  is further compared against the EP of a squeezed vacuum state (black), whose degree of squeezing is selected in accord with the asymptotic distillation of squeezing available for the corresponding trilinear state.

Fig. 2 achieves at least the value of  $\mathcal{E}_b$ . This persists even though residual LN is generated with the thermal pump mode ( $\mathcal{L}_{a:c}$  and  $\mathcal{L}_{a:b}$ ) and is subsequently traced out. The Gaussian entanglement, extracted from the covariance matrix of the state, is always zero during the evolution, indicating that the thermally induced entanglement involves correlations beyond the covariance matrix.

To illustrate the robustness of these phenomena we examined the deviation of mode  $b$  from the ideal ground state. Thermal occupation of mode  $b$ , while reducing the absolute value of the EP, maintains the enhancement of nonclassicality due to increasing the thermal energy in  $a$  (see SM). Remarkably, this occurs even when the thermal occupation of  $b$  is greater than 1 and can occur when greater than  $\bar{n}$ . This allows experimental tests of these phenomena without being bound to the ground state of mode  $b$ . Additionally, we examined the effect on the EP and LN when the trilinear interaction occurs outside the RWA, so that the free evolution of the oscillators contributes (see SM). While the EP is robust to these effects, the LN decreases greatly, while still retain-

ing the property that it increases with  $\bar{n}$ . Finally we also examined the effect of coupling the modes to a thermal environment. While both EP and LN are reduced by the interaction with the environment, significant values of both quantities remain (see SM).

*Higher Order Nonlinearities*— It is possible that higher nonlinearities will exhibit different phenomena and so we examine highly nonlinear Hamiltonians of the form  $H_{\text{NL}} \propto a(b^\dagger)^N + a^\dagger b^N$ , where  $N > 2$ . Continuing the logic, the internal thermal driving of  $a$  will drive higher order quanta splitting, resulting in generalised squeezing [16] in  $b$  and producing highly nonclassical and non-Gaussian states with large entanglement potential.

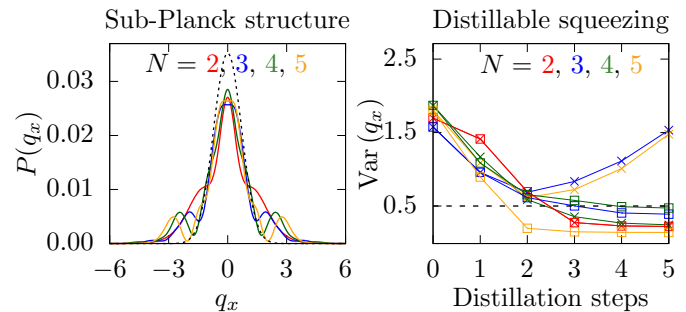


Figure 3. (a) The probability densities  $P(q_x)$  from  $H_{\text{NL}} = \Omega_T(a^\dagger b^N + ab^\dagger)^N$  with  $N = 2$  (red), 3 (blue), 4 (green) and 5 (yellow) are compared at the optimal time (see text), compared with the ground state distribution (dashed black). (b) Universal (squares) and non-universal (crosses) squeezing distillation as a function of number of copies of the state. For odd  $N$  the universal method does not find distillable squeezing around the global maximum of the distribution, unlike the case of even  $N$ . Instead, the non-universal method searches the whole distribution for nonclassical structures and distills them to find distillable squeezing. In both panels mode  $a$  is initially in a thermal state with  $\bar{n} = 1$  and mode  $b$  is in the ground state.

In Fig. 3 we show the probability densities in  $q_x$  for the nonclassical states produced by these higher order nonlinearities. They are clearly non-Gaussian, with embedded sub-Planck structures. However the distillable squeezing shows features distinct from the  $N = 2$  case considered above. The universal method of distillation [25], which extracts nonclassical features from the curvature around the global maximum of the distribution, does not produce squeezing for odd  $N$ . Indeed this is reflected in the distributions which have low curvature around their maxima. Instead the non-universal method [25, 31], which optimises the distillation around arbitrary features of the distribution, can extract squeezing even from the odd parity Hamiltonians. By measuring the copies in the distillation around sub-Planck features in the distribution, optimising the measurement at each distillation step, distillable squeezing, and thus nonclassicality, can still be detected. However the distillable squeezing found through the non-universal method does not increase with  $\bar{n}$ , in contrast

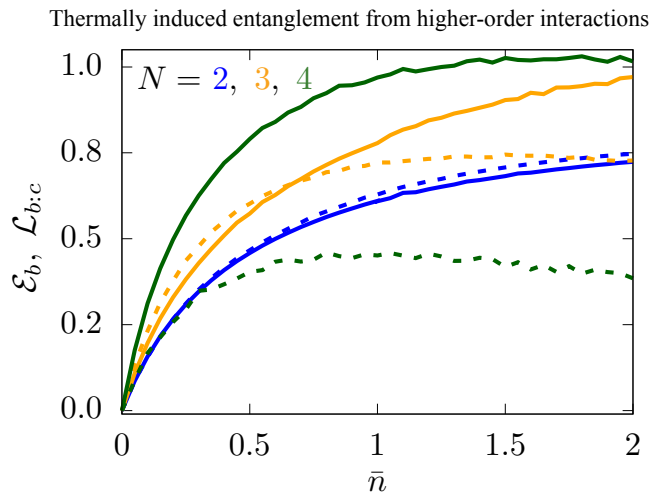


Figure 4. Entanglement potential  $\mathcal{E}_b$  (solid curves) and  $\mathcal{L}_{b,c}$  (dashed curves) generated by incoherent thermal noise in  $a$  for Hamiltonians  $H_{NL}$ . The evolution times and coupling strengths are as previously described in the main text. The entanglement extracted by the auxiliary linear coupling ceases to closely follow the EP for  $N > 2$ .

with the universal method analysed in detail in Fig 1.

This nonclassicality can again be used to generate entanglement. Fig. 4 shows the entanglement potential and logarithmic negativity via coupling to an auxiliary state for various  $N$ . Increasing  $N$  tends to increase the nonclassicality generated by the same thermal energy, however, similar to the failure of universal squeezing distillation, the anticipated generation of entanglement via linear coupling in parallel with the generation of nonclassicality eventually fails to reach the EP for larger values of  $\bar{n}$ . For  $N = 3$ , replacing the linear coupling with a trilinear coupling does not improve  $\mathcal{L}_{b,c}$ . This suggests that among these the trilinear Hamiltonian of Eq. (4), combined with a linear coupling to another mode, is the most effective in terms of generating non-Gaussian entanglement from small thermal energy.

*Discussion*— We have singled out the simplest nonlinearity coupling linear oscillators, the degenerate trilinear interaction, combined with a linear coupling in order to transmute the thermal energy of a few quanta into greater nonclassicality and non-Gaussian entanglement. Other possibilities among three mode interactions are surprisingly limited in their capacity to generate bipartite entanglement [6, 22] (see SM). That larger thermal fluctuations are converted into increasing coherent quantum phenomena, such as entanglement [32–35], detected by logarithmic negativity, functions as a direct proof of genuine nonlinear quantum effects, as it cannot happen for linearised dynamics within the Gaussian approximation provided by the covariance matrix. While such dynamics intrinsically involves higher than quadratic interac-

tion terms, and shows quantum non-Gaussian effects [18] such a direct experimental proof is yet to be demonstrated. In the past, such features were predicted in systems taking advantage of discrete nonlinearities in the level structure of atoms or superconducting circuits with very strong saturation [34–36] while here entanglement materialises without the direct use of saturation in such discrete nonlinearities. It is also conceptually different to thermally induced entanglement using controlled-SWAP gates [37, 38].

This proposal, inspired by recent experimental achievements regarding trilinear interactions in trapped ion [18–20] and superconducting circuit platforms [10, 17], provides a clear example of the hidden power of multimode nonlinear systems to achieve, autonomously and unconditionally, increasing nonclassical quantum behaviour leveraging only small thermal energy. Furthermore, the linear coupling required to directly test the parallel generation of entanglement has already been proposed for optical systems [39] and is likely to be easily adapted to phononic systems and superconducting circuits.

#### ACKNOWLEDGEMENTS

The authors acknowledge funding from Project 21-13265X of the Czech Science Foundation. This project has received funding from the European Union’s 2020 research and innovation programme (CSA—Coordination and support action, H2020-WIDESPREAD-2020-5) under grant agreement No. 951737 (NONGAUSS).

\* [pradip.laha@upol.cz](mailto:pradip.laha@upol.cz)

† [darren.moore@upol.cz](mailto:darren.moore@upol.cz)

‡ [filip@optics.upol.cz](mailto:filip@optics.upol.cz)

- [1] S. L. Braunstein and P. van Loock, *Rev. Mod. Phys.* **77**, 513 (2005).
- [2] N. B. Grosse, S. Assad, M. Mehmet, R. Schnabel, T. Symul, and P. K. Lam, *Phys. Rev. Lett.* **100**, 243601 (2008).
- [3] M. K. Olsen, *Phys. Rev. A* **97**, 033820 (2018).
- [4] V. Boyer, A. M. Marino, R. C. Pooser, and P. D. Lett, *Science* **321**, 544 (2008).
- [5] A. S. Coelho, F. A. S. Barbosa, K. N. Cassemiro, A. S. Villar, M. Martinelli, and P. Nussenzweig, *Science* **326**, 823 (2009).
- [6] E.-A. R. González, A. Borne, B. Boulanger, J.-A. Levenson, and K. Bencheikh, *Phys. Rev. Lett.* **120**, 043601 (2018).
- [7] C. Silberhorn, P. K. Lam, O. Weiß, F. König, N. Korolkova, and G. Leuchs, *Phys. Rev. Lett.* **86**, 4267 (2001).
- [8] C. Gabriel, A. Aiello, W. Zhong, T. G. Euser, N. Y. Joly, P. Banzer, M. Förtsch, D. Elser, U. L. Andersen, C. Marquardt, P. S. J. Russell, and G. Leuchs, *Phys. Rev. Lett.* **106**, 060502 (2011).

- [9] M. Perelshtein, K. Petrovnin, V. Vesterinen, S. H. Raja, I. Lilja, M. Will, A. Savin, S. Simbierowicz, R. Jabdaraghi, J. Lehtinen, L. Grönberg, J. Hassel, M. Prunnila, J. Govenius, S. Paraoanu, and P. Hakonen, [arXiv:2111.06145 \[quant-ph\]](#) (2021).
- [10] C. W. S. Chang, C. Sabín, P. Forn-Díaz, F. Quijandría, A. M. Vadiraj, I. Nsanzineza, G. Johansson, and C. M. Wilson, *Phys. Rev. X* **10**, 011011 (2020).
- [11] N. E. Frattini, U. Vool, S. Shankar, A. Narla, K. M. Sliwa, and M. H. Devoret, *Appl. Phys. Lett.* **110**, 222603 (2017).
- [12] F. Quijandría, G. Johansson, A. Ferraro, S. Gasparinetti, G. Ferrini, and T. Hillmann, *Phys. Rev. Lett.* **125**, 160501 (2020).
- [13] D. Leibfried, R. Blatt, C. Monroe, and D. Wineland, *Rev. Mod. Phys.* **75**, 281 (2003).
- [14] T. G. Tiecke, J. D. Thompson, N. P. de Leon, L. R. Liu, V. Vuletić, and M. D. Lukin, *Nature* **508**, 241 (2014).
- [15] X. R. Nie, C. F. Roos, and D. F. V. James, *Phys. Lett. A* **373**, 422 (2009).
- [16] S. L. Braunstein and R. I. McLachlan, *Phys. Rev. A* **35**, 1659 (1987).
- [17] A. Vrajitoarea, Z. Huang, P. Groszkowski, J. Koch, and A. A. Houck, *Nat. Phys.* **16**, 211 (2020).
- [18] S. Ding, G. Maslennikov, R. Hablützel, H. Loh, and D. Matsukevich, *Phys. Rev. Lett.* **119**, 150404 (2017).
- [19] S. Ding, G. Maslennikov, R. Hablützel, and D. Matsukevich, *Phys. Rev. Lett.* **121**, 130502 (2018).
- [20] G. Maslennikov, S. Ding, R. Hablützel, J. Gan, A. Roulet, S. Nimmrichter, J. Dai, V. Scarani, and D. Matsukevich, *Nat. Commun.* **10**, 202 (2019).
- [21] Z. Y. Ou, S. F. Pereira, H. J. Kimble, and K. C. Peng, *Phys. Rev. Lett.* **68**, 3663 (1992).
- [22] A. Agustí, C. W. S. Chang, F. Quijandría, G. Johansson, C. M. Wilson, and C. Sabín, *Phys. Rev. Lett.* **125**, 020502 (2020).
- [23] D. N. Klyshko, *Phys. Lett. A* **213**, 7 (1996).
- [24] L. Innocenti, L. Lachman, and R. Filip, *npj Quantum Inf.* **8**, 1 (2022).
- [25] R. Filip, *Phys. Rev. A* **88**, 063837 (2013).
- [26] C. Marquet, F. Schmidt-Kaler, and D. James, *Appl. Phys. B* **76**, 199 (2003).
- [27] A. Lemmer, *Quantum dynamics with trapped ions*, Dissertation, Universität Ulm (2018).
- [28] W. H. Zurek, *Nature* **412**, 712 (2001).
- [29] J. K. Asbóth, J. Calsamiglia, and H. Ritsch, *Phys. Rev. Lett.* **94**, 173602 (2005).
- [30] M. B. Plenio, *Phys. Rev. Lett.* **95**, 090503 (2005).
- [31] R. Filip and P. Zapletal, *Phys. Rev. A* **90**, 043854 (2014).
- [32] S. Bose, I. Fuentes-Guridi, P. L. Knight, and V. Vedral, *Phys. Rev. Lett.* **87**, 050401 (2001).
- [33] M. S. Kim, J. Lee, D. Ahn, and P. L. Knight, *Phys. Rev. A* **65**, 040101 (2002).
- [34] P. Marek, L. Lachman, L. Slodička, and R. Filip, *Phys. Rev. A* **94**, 013850 (2016).
- [35] P. Laha, L. Slodička, D. W. Moore, and R. Filip, *Opt. Express* **30**, 8814 (2022).
- [36] L. Slodička, P. Marek, and R. Filip, *Opt. Express* **24**, 7858 (2016).
- [37] R. Filip, M. Dušek, J. Fiurášek, and L. Mišta, *Phys. Rev. A* **65**, 043802 (2002).
- [38] Y. Y. Gao, B. J. Lester, K. S. Chou, L. Frunzio, M. H. Devoret, L. Jiang, S. M. Girvin, and R. J. Schoelkopf, *Nature* **566**, 509 (2019).
- [39] S. Krastanov, M. Heuck, J. H. Shapiro, P. Narang, D. R. Englund, and K. Jacobs, *Nat. Commun.* **12**, 191 (2021).
-

## SUPPLEMENTARY MATERIAL

### NON-GAUSSIAN ENTANGLEMENT VIA SPLITTING OF A FEW THERMAL QUANTA

#### Nondegenerate and Multiple Trilinear Hamiltonians

In the main analysis, we focused on degenerate trilinear coupling as the best candidate for the generic entanglement generation from a few thermal quanta. Alternative configurations of trilinear Hamiltonians are briefly analysed here and demonstrated to be inefficient in producing entanglement. In the nondegenerate case, the Hamiltonian is given by

$$H^{\text{ND}} = \Omega(a^\dagger b c + a b^\dagger c^\dagger), \quad (\text{S1})$$

where  $\Omega$  is the coupling strength. This interaction Hamiltonian has already been realised using three  $^{171}\text{Yb}^+$  ions in a Paul trap, where  $a$  corresponds to the axial mode, and  $b$  and  $c$  to the two radial modes [19]. Thermally pumping any one of the modes  $a$ ,  $b$ ,  $c$ , does not produce entanglement among the remaining pair. However, we can check the EP of these modes individually and extract the entanglement via continuous linear coupling to an auxiliary mode  $d$ . Setting  $\tau = \Omega t$  as before, and studying the induced nonclassicality in mode  $b$  (equivalent to  $c$  by symmetry) by thermally driving mode  $a$ , while both modes  $b$  and  $c$  are initially in their respective ground states we find (Fig. S1) that EP can be generated in mode  $b$  ( $c$ ), in negligible quantities compared to the degenerate case analysed in the main text. As before, we also see that the nonclassicality converted from the thermal noise resource can be leveraged via coupling  $b$  to an auxiliary mode  $d$  (i.e.  $H_{\text{aux}}^{\text{ND}} = H^{\text{ND}} + g(bd^\dagger + b^\dagger d)$ , or similarly with  $c$ ) to create entanglement which follows the behavior of  $\mathcal{E}_b$  ( $\mathcal{E}_c$ ). Again we set  $g = \Omega$ . We note that  $\mathcal{E}_a$  is greater than  $\mathcal{E}_b$  (or equivalently,  $\mathcal{E}_c$ ) which is not the case for the degenerate case investigated in the main text.

Alternatively, multiple trilinear interactions with one common mode are described by the following Hamiltonians,

$$H_1 = \Omega_1(ab^{\dagger 2} + a^\dagger b^2) + \Omega_2(cb^{\dagger 2} + c^\dagger b^2) \quad (\text{S2})$$

$$H_2 = \Omega_1(ab^{\dagger 2} + a^\dagger b^2) + \Omega_2(ac^{\dagger 2} + a^\dagger c^2). \quad (\text{S3})$$

In Fig. S2 we show the behavior of  $\mathcal{L}_{b,c}$  for  $H_1$  (olive) and  $H_2$  (green). In both the cases the induced entanglement is much smaller compared to  $\mathcal{L}_{b,c}$  of the individual interaction given by Eq. (4).

#### Coherent and Incoherent Internal Driving

In the main text we focus on the incoherent resource of thermal states to generate coherent quantum phenomena.

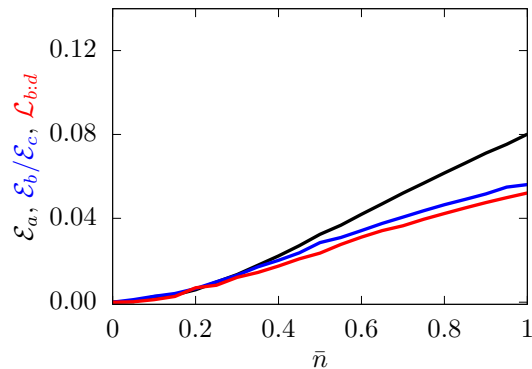


Figure S1. EP of mode  $a$  (black), and identical modes  $b$  and  $c$  (blue) are plotted as a function of  $\bar{n}$  for the nondegenerate trilinear system given in Eq.(S1).  $a$  is prepared in a thermal state characterised by  $\bar{n}$  while  $b$  and  $c$  are in the ground state. Adding a linear coupling between mode  $b$  and an auxiliary mode  $d$ , as in  $H_{\text{aux}}^{\text{ND}}$ , the LN  $\mathcal{L}_{b:d}$  increases with  $\bar{n}$  but is negligible compared to the degenerate case.

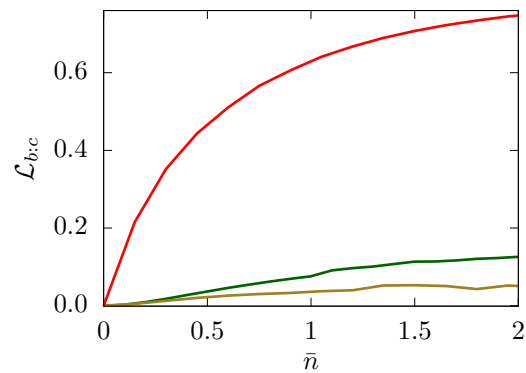


Figure S2.  $\mathcal{L}_{b,c}$  for  $H_1$  (olive),  $H_2$  (green) is compared with  $\mathcal{L}_{b,c}$  for  $H$  (red) in Fig. 2. The LN for multiple trilinear interactions is much smaller than for the single degenerate version preferred in the main text.

With coherent resources the amount of nonclassicality generated can be greatly increased, interestingly however the qualitative behaviour can already be observed for the thermal states.

In Fig. S3 we show the EP and LN with  $a$  prepared in a coherent state (solid circles)  $|\alpha\rangle$  with  $|\alpha|^2 = \bar{n}$ . This is much greater than that achievable with thermal states (solid lines). If the phase is uncertain then the state has Poissonian noise in the Fock basis, and we obtain the

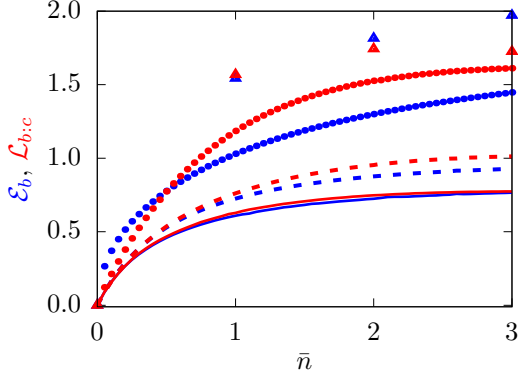


Figure S3. The role of different initial states on the entanglement production.  $\mathcal{E}_b$  (blue) and  $\mathcal{L}_{b;c}$  (red) are calculated using different resources to drive  $a$ . Represented are the thermal states (solid lines), coherent states (solid circles), Poissonian noise (dashed) and Fock states (solid triangles).  $b$  is always initialised in the ground state. Note that for coherent states and Poissonian noise we have  $\bar{n} = |\alpha|^2$ .

phase randomised coherent states (PRCS) defined by

$$\frac{1}{2\pi} \int_0^{2\pi} d\theta |\alpha e^{i\theta}\rangle \langle \alpha e^{i\theta}| = e^{-|\alpha|^2} \sum_{n=0}^{\infty} \frac{|\alpha|^{2n}}{n!} |n\rangle \langle n|. \quad (\text{S4})$$

Here, it is instructive to compare with less noisy and more coherent drives under the same conditions. Poissonian noise (dashed lines) produces less nonclassicality and entanglement than the coherent state, but more than the thermal states. Furthermore, the Fock states, which have zero noise around the phonon number and no quantum coherence, but are extremely nonclassical, induce larger nonclassicality than the other examples provided.

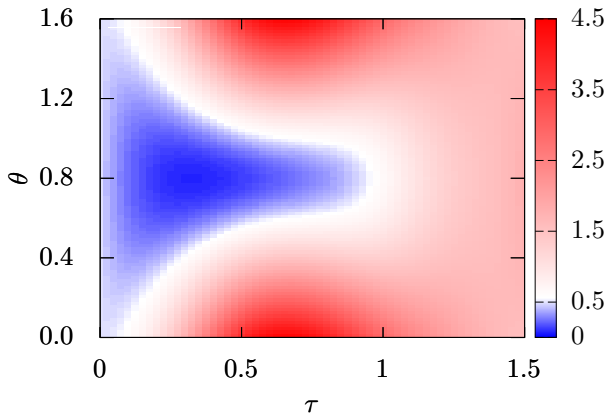


Figure S4. The variance of the generalised quadrature  $X_\theta$  of mode  $b$  as a function of scaled time  $\tau = \Omega_T t$  and phase  $\theta$ , when  $a$  is driven coherently (with strength  $\bar{n} = |\alpha|^2 = 3$ ).

If mode  $a$  is prepared in a coherent state then the nonclassical state prepared in  $b$  is phase sensitive, in contrast with that generated by thermal energy, with the phase

determined by the phase of the coherent state. For large  $\alpha$  the mode  $a$  in the trilinear Hamiltonian can be approximated with the c-number  $\alpha = |\alpha|e^{i\phi}$  as

$$H \sim \alpha(b^\dagger)^2 + \alpha^* b^2 = |\alpha| (b^{\dagger 2} e^{i\phi} + b^2 e^{-i\phi}). \quad (\text{S5})$$

The coherent phase  $\phi$  can be connected with the quadrature angle  $\frac{\theta}{2}$  via  $\phi = \theta - \frac{\pi}{2}$ , so that the Hamiltonian takes the standard squeeze operator form

$$H = -i|\alpha| (b^{\dagger 2} e^{i\theta} - b^2 e^{-i\theta}). \quad (\text{S6})$$

Fig. S4 shows the squeezing in the generalised quadrature  $X_\theta = \frac{1}{\sqrt{2}} (b e^{-i\frac{\theta}{2}} + b^\dagger e^{i\frac{\theta}{2}})$  for the coherent state with  $|\alpha|^2 = \bar{n} = 3$  and  $\phi = 0$ . The squeezing is most manifest along the quadrature axis defined by  $\theta = \frac{\pi}{2}$ , in accordance with the prediction of the saturated trilinear system. In contrast, for a phase random initial state such as a thermal state or PRCS, the nonclassicality is phase insensitive.

### Influence of the Environment

In our treatment of the trilinear dynamics we have assumed unitary evolution due to the high quality of the dynamics and sufficient decoupling from the environment for both trapped ions and superconducting circuits over time required for such experiments. In this Section, we detail our numerical observations on the robustness of the thermally induced entanglement generation against such effects. If we ignore the contributions of the Lamb shift leading to a small renormalization of the system energy levels, the Lindblad master equation describing such environmental effects is given by

$$\frac{d\rho_S}{dt} = -i[H, \rho_S] + \sum_k \left( L_k \rho_S L_k^\dagger - \frac{1}{2} [\rho_S, L_k^\dagger L_k] \right). \quad (\text{S7})$$

Here,  $\rho_S(t)$  is the reduced density matrix of the system. The operators  $L_k = \sqrt{\lambda_k} A_k$  are the Lindblad jump operators, and the environment couples to the system through the operators  $A_k$  with coupling rates  $\lambda_k$ . For the two mechanical modes coupled to the environment with same temperature  $n_{\text{th}}$ , we have the Lindblad operators ( $L_k$ 's) given by  $\sqrt{\lambda_a(1 + \bar{n}_{\text{th}})} a$ ,  $\sqrt{\lambda_a \bar{n}_{\text{th}}} a^\dagger$ , and  $\sqrt{\lambda_b(1 + \bar{n}_{\text{th}})} b$ ,  $\sqrt{\lambda_b \bar{n}_{\text{th}}} b^\dagger$ . When considering the LN there are additional terms for the mode  $c$  involved in the linear coupling.

In Fig. S5 the effect of decoherence on both the EP and LN is examined in terms of the strength of the coupling to the environment. The system evolves with mode  $a$  in a thermal state with  $\bar{n} = 2$  and the remaining modes in the ground state, until a fixed time set by the unitary evolution in the main text. Both quantities experience a sharp

decay to zero with similar behaviour, with the rate increasing with the temperature of the environment. However in Fig. S6 the direct evolution against time shows that while the nonclassicality is largely reduced, significant quantities are still visible, albeit at slightly shorter times.

Importantly, as explained in the following section, the enhancement due to initial thermal noise remains visible despite the reduction in logarithmic negativity.

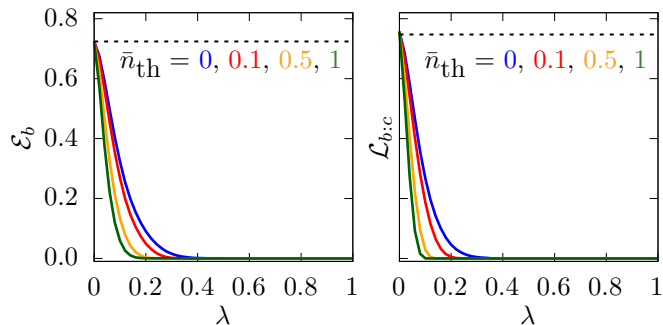


Figure S5. Effect of environmental induced decoherence on  $\mathcal{E}_b$  and  $\mathcal{L}_{b:c}$  when all modes are connected to the same thermal bath with different temperatures  $\bar{n}_{\text{th}} = 0$  (blue), 0.1 (red), 0.5 (yellow), and 1.0 (green). Initially,  $a$  is in a thermal state with  $\bar{n} = 2$ , and  $b$  and  $c$  are in the ground states. The black dashed lines represents the unitary evolution ( $\lambda = 0$ ). We fix the time as the optimised time of the unitary case, as described in the main text.

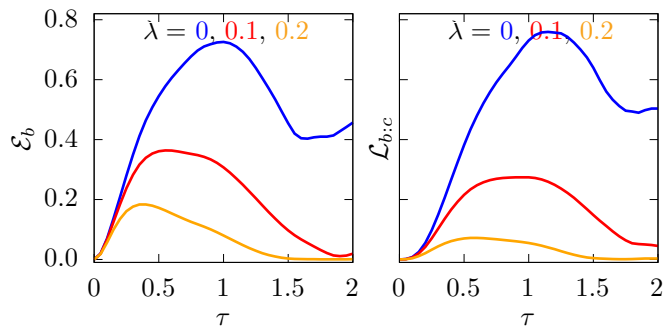


Figure S6. Effect of environmental induced decoherence on  $\mathcal{E}_b$  and  $\mathcal{L}_{b:c}$  when all modes are connected to the same bath with  $\bar{n}_{\text{th}} = 0$ . Initially,  $a$  is in a thermal state with  $\bar{n} = 2$ , and  $b$  and  $c$  are in the ground state. We fix the time as the optimised time of the unitary case, as described in the main text.

### Thermal Occupation of the Radial Mode

In our analysis of the nonclassicality and EP for the trilinear system we assumed the idealisation that mode  $b$  is prepared in the ground state with the only thermal energy in mode  $a$ . This is because both trapped ions experiments and superconducting circuits can achieve good

ground states of these modes. However, to check the stability outside this limit we now briefly consider the effect of thermal occupation of modes  $b$  and  $c$ . Advantageously, the thermally induced effects persist even if the thermal energy in mode  $b$ , characterised by an average occupation  $\bar{n}_b$ , is greater than 1. Fig. S7 shows a recreation of Fig. 1 from the main text with  $\bar{n}_b = 1.5$ . The clear demonstration of nonclassicality from the phonon statistics in Fig. 1 is lost however Klyshko's criteria still verify nonclassicality. Similarly, the distillable squeezing in  $q_x$  can still be reduced below the shot noise by very large thermal energy in  $a$ .

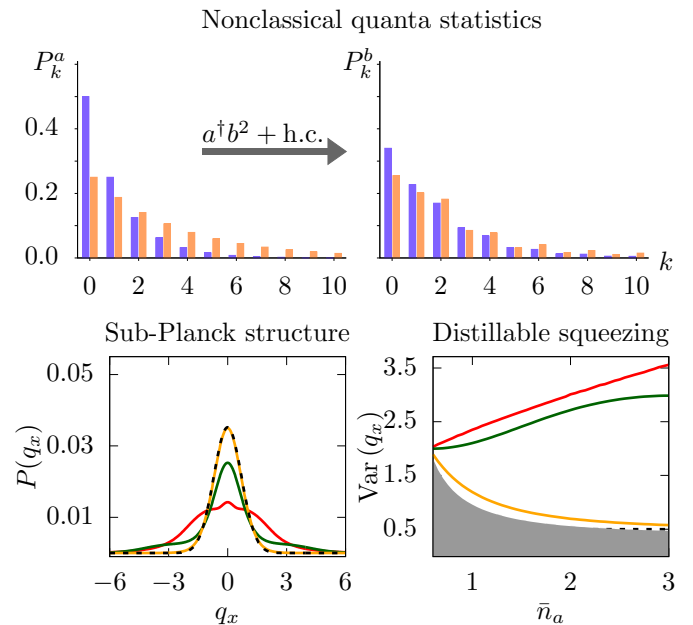


Figure S7. Analysis of the nonclassicality in mode  $b$  as in Fig. 1 with  $\bar{n}_b = 1.5$ . The clear visual generation of nonclassicality by the occupation of only even Fock states is lost, however Klyshko's criteria still indicate nonclassicality. The distillable squeezing can also still achieve values below the shot noise by preparing  $a$  in thermal states with  $\bar{n}_a > 3$ .

In Fig. S8 we show how the distillable squeezing varies as a function of  $\bar{n}_b$ . The amount of thermal energy in  $a$  required to see reduction in the position variance below the shot noise increases with  $\bar{n}_b$ , however it is still possible to see nonclassicality even for large values of  $\bar{n}_b$ .

Finally in Fig. S9 we also show the EP as a function of  $\bar{n}_b$ . Increasing  $\bar{n}_b$  (Fig S9) drastically decreases the absolute value of the EP. However our main result, that the EP is increased by increasing the thermal energy in mode  $a$ , is still visible up to saturation at  $\bar{n} \approx 3$ .

### Effect of Free Motion on Nonclassicality and Entanglement

Our analysis takes place in a frame of reference that eliminates the free motion of the component oscillators,

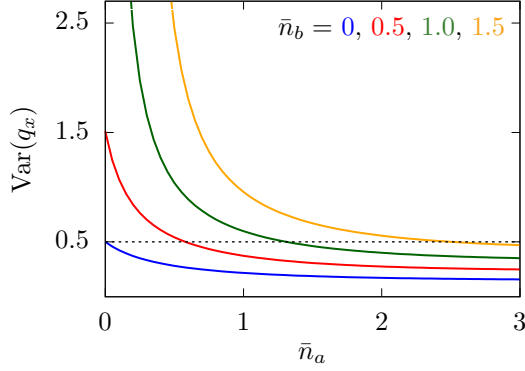


Figure S8. Universal distillable squeezing when mode  $b$  deviates from the ideal ground state configuration to a thermal state with average phonon number  $\bar{n}_b = 0$  (blue), 0.5 (red), 1 (green) and 1.5 (yellow) as a function of  $\bar{n}_a$ . The distillable squeezing indicates nonclassicality for large enough thermal energy in  $a$ .

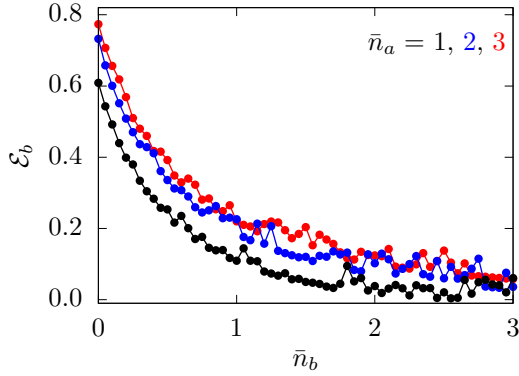


Figure S9.  $\mathcal{E}_b$  as a function of the thermal occupation  $\bar{n}_b$  of the radial mode  $b$  for several values of  $\bar{n}_a$ . While the overall effect is to reduce the amount of EP produced, the EP is still visibly increased by an increase in the thermal occupation of mode  $a$ .

which is suited to the platforms of trapped ions that we

consider as well as similar systems such as superconducting circuits. If such trilinear Hamiltonians occur in a context in which such transformations cannot be performed then the effect of the free motion must be taken into account. The Hamiltonian, including the linear coupling required to study the LN, is modified to

$$H_{\text{FM}} = \sum_{k=a,b,c} \omega_k k^\dagger k + \Omega_T (a^\dagger b^2 + ab^{\dagger 2}) + g(b^\dagger c + bc^\dagger). \quad (\text{S8})$$

We therefore briefly verify if the observed effects qualitatively persist if the free evolution is present. As in the main text, we select  $\Omega_T = g$ . Due to energy conservation, there is only one parameter for the frequency, as  $\omega_a = 2\omega_b = 2\omega_c$ . While the effects of free motion terms are typically destructive to quantum phenomena, here we find that the EP is in fact quite resilient to these effects but the LN suffers as shown in Fig S10. We note however

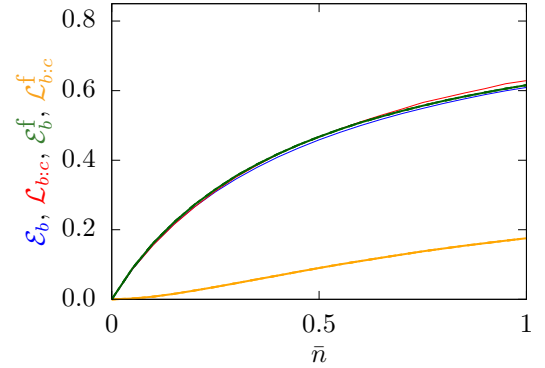


Figure S10. The entanglement potential and logarithmic negativity in the presence of free motion. Blue and red correspond to the EP and LN analysed in Fig. 2 of the main text. The green and yellow correspond to the nonclassicality and entanglement dynamics involving the free motion.

that LN is still thermally stimulated and reaches observable values for experimental tests within this regime.